

# Vegetation Phenology in Permafrost Regions of Northeastern China Based on MODIS and Solar-induced Chlorophyll Fluorescence

WEN Lixiang<sup>1</sup>, GUO Meng<sup>1</sup>, YIN Shuai<sup>2</sup>, HUANG Shubo<sup>1</sup>, LI Xingli<sup>1</sup>, YU Fangbing<sup>1</sup>

(1. Key Laboratory of Geographical Processes and Ecological Security in Changbai Mountains, Ministry of Education, School of Geographical Sciences, Northeast Normal University, Changchun 130024, China; 2. Centers for Global Environmental Research, National Institute for Environmental Studies, Tsukuba 305-8555, Japan)

**Abstract:** Vegetation phenology is an indicator of vegetation response to natural environmental changes and is of great significance for the study of global climate change and its impact on terrestrial ecosystems. The normalized difference vegetation index (NDVI) and enhanced vegetation index (EVI), extracted from the Moderate Resolution Imaging Spectrometer (MODIS), are widely used to monitor phenology by calculating land surface reflectance. However, the applicability of the vegetation index based on ‘greenness’ to monitor photosynthetic activity is hindered by poor observation conditions (e.g., ground shadows, snow, and clouds). Recently, satellite measurements of solar-induced chlorophyll fluorescence (SIF) from OCO-2 sensors have shown great potential for studying vegetation phenology. Here, we tested the feasibility of SIF in extracting phenological metrics in permafrost regions of the northeastern China, exploring the characteristics of SIF in the study of vegetation phenology and the differences between NDVI and EVI. The results show that NDVI has obvious SOS advance and EOS lag, and EVI is closer to SIF. The growing season length based on SIF is often the shortest, while it can represent the true phenology of vegetation because it is closely related to photosynthesis. SIF is more sensitive than the traditional remote sensing indices in monitoring seasonal changes in vegetation phenology and can compensate for the shortcomings of traditional vegetation indices. We also used the time series data of MODIS NDVI and EVI to extract phenological metrics in different permafrost regions. The results show that the length of growing season of vegetation in predominantly continuous permafrost (zone I) is longer than in permafrost with isolated taliks (zone II). Our results have certain significance for understanding the response of ecosystems in cold regions to global climate change.

**Keywords:** vegetation phenology; permafrost; Moderate Resolution Imaging Spectrometer (MODIS); solar-induced chlorophyll fluorescence (SIF); northeastern China

**Citation:** WEN Lixiang, GUO Meng, YIN Shuai, HUANG Shubo, LI Xingli, YU Fangbing, 2021. Vegetation Phenology in Permafrost Regions of Northeastern China Based on MODIS and Solar-induced Chlorophyll Fluorescence. *Chinese Geographical Science*, 31(3): 459–473. https://doi.org/10.1007/s11769-021-1204-x

## 1 Introduction

Vegetation phenology, the timing of seasonal developmental stages in plant life cycles, has gained more and more public and scientific attention in the past few decades because of its sensitivity to climate change and

consequences for ecosystem function (Tang et al., 2016). By controlling the seasonal activity of vegetation and physiological processes such as photosynthesis, changes in vegetation phenology can have a fundamental impact on the entire ecosystem. Consequently, accurate measurements of vegetation phenology are vital for the in-

Received date: 2020-11-02; accepted date: 2021-03-01

Foundation item: Under the auspices of National Key Research and Development Projects (No. 2018YFE0207800), National Natural Science Foundation of China (No. 41871103)

Corresponding author: GUO Meng. E-mail: [guom521@nenu.edu.cn](mailto:guom521@nenu.edu.cn)

© Science Press, Northeast Institute of Geography and Agroecology, CAS and Springer-Verlag GmbH Germany, part of Springer Nature 2021

depth study of terrestrial ecosystems (Cleland et al., 2007; Bradley et al., 2011; Richardson et al., 2012; Wu et al., 2013). The northeastern permafrost regions, located in the southern fringe of the Eurasian permafrost, is the only high-latitude permafrost region in China and is highly sensitive to global climate change (Wei et al., 2011). Therefore, studying the vegetation phenology in this area is of great significance for understanding the response of ecosystems in cold regions to global climate change.

Over the past few decades, satellite remote sensing has been widely used to monitor vegetation phenology (Justice et al., 1985; Piao et al., 2007). It is usually achieved using vegetation indices (VIs), which are a combination of the reflectance of different spectral bands, aimed at enhancing the sensitivity to green vegetation (Huete et al., 2002). Normalized difference vegetation index (NDVI) and enhanced vegetation index (EVI) are the primary indicators used to estimate the start and end of the growing season (SOS, EOS) at regional and global scales (Myneni et al., 1997; Delbart et al., 2006; Shen et al., 2014; Deng et al., 2019). However, various factors can reduce the accuracy of NDVI or EVI estimation of vegetation phenology, such as the interference of ground shadows, snow and other backgrounds, poor atmospheric conditions, and application in different vegetation types. For example, Hmimina et al. (2013) monitored the seasonal dynamics of different types of vegetation cover using the medium resolution imaging spectrometer (MODIS) NDVI and found that NDVI can not accurately infer the phenological patterns of evergreen forests. Wu et al. (2014) found that NDVI and EVI had limited ability to track phenology in the growing season of evergreen coniferous forest ecosystems. Moreover, in deciduous forests, trees are usually greened later than the herbs and shrubs, which means that the greening date determined by the remote sensing index may reflect the greening date of the herbs and shrubs, rather than the dominant trees (Fu et al., 2014).

As a supplement to the vegetation indices, solar-induced chlorophyll fluorescence (SIF) provides new possibilities for monitoring plant functions from space (Guanter et al., 2014). Traditional remote sensing indices monitor vegetation based on changes in vegetation 'greenness', while SIF is directly related to actual plant photochemical reactions. Therefore, SIF has a stronger physiological basis than traditional vegetation

indices (Meroni et al., 2009; Zarco-Tejada et al., 2013). SIF is essentially the energy flux emitted by plant chlorophyll molecules after absorbing sunlight in the wavelength range of 600–800 nm (Baker, 2008). The absorption of light energy by chlorophyll molecules is mainly used in three processes: photochemical reactions in photosynthesis, heat loss, and heat emission in the form of long waves. The third process comprises SIF, which is less than 5% of the light energy absorbed by plants; however, it provides a more direct method of measuring photosynthesis activities than similar approaches (Baker, 2008; Frankenberg et al., 2011; Köhler et al., 2018). As inversion accuracy of carbon observation satellites has continued to develop, such as the Greenhouse Gases Observing Satellite (GOSAT) and Orbiting Carbon Observatory 2 (OCO-2), we can monitor chlorophyll fluorescence across the globe (Guanter et al., 2012; 2014; Lee et al., 2013), showing the great potential of using SIF to advance research on phenology. However, the current research on SIF mainly focuses on the analysis of the consistency between SIF and GPP and the comparison of SIF with other indices during the growth season (Joiner et al., 2011; 2014; Walther et al., 2016; Wang et al., 2020), rather than using SIF to calculate phenological values. Moreover, most of the previous studies were on the global scale or a large regional scale. However, as the spatial resolution changes, the relationship between SIF and vegetation index also changes (Guo et al., 2020).

Some studies indicate that with the increase in global temperature, the vegetation phenology in high latitudes of the northern hemisphere shows trends of early spring and late autumn (Myneni et al., 1997; Richardson et al., 2013). However, due to the stress of non-biophysical factors (such as temperature, precipitation, and soil moisture), changes in vegetation phenology exhibit a complex spatial and temporal pattern (Zhou, 2020). The vegetation in the permafrost regions of northeastern China is characterized by obvious seasonality, high vegetation coverage, and relatively homogeneous types, making it an ideal area to study vegetation growth processes and phenological changes based on satellite monitoring (Yu and Zhuang, 2006). However, there are few reports on the study of vegetation phenology in this area, especially from the perspective of permafrost zoning. This study selected the permafrost regions of northeastern China as a test bed to 1) explore the feasibility

of SIF in extracting phenological metrics in a small area; 2) compare the ability of SIF, NDVI, and EVI in monitoring phenology; and 3) investigate temporal and spatial patterns of vegetation phenology at the pixel-scale in permafrost regions of the northeastern China.

## 2 Materials and Methods

### 2.1 Study region

The study region is located in the northeastern China (46°30'N–53°30'N, 115°52'E–135°09'E), spanning Inner Mongolia and northern Heilongjiang Province, and connecting Russia and Mongolia, with an area of approximately  $3.8 \times 10^5 \text{ km}^2$  (Fig. 1). This area has a continental climate associated with cold temperate zones, with long and dry winters and short and humid summers. The average annual temperature is  $-5^\circ\text{C}$ – $2^\circ\text{C}$ , and the annual precipitation is 260–600 mm (Mao et al., 2012). The western part of the study area is the Hulun Buir Plateau, the eastern part of the study area is the Xiao Hinggan Mountains, the Da Hinggan Mountains are located in the middle of the study area oriented northeast-southwest, and between the Da Hinggan Mountains and Xiao Hinggan Mountains is the Songnen Plain.

The entire study area is divided into three parts: predominantly continuous permafrost (zone I), permafrost with isolated taliks (zone II), and isolated permafrost

(zone III) (Mi, 1990). The thickness of permafrost in zone I, zone II and zone III are 50–100 m, 20–50 m and 5–20 m respectively. The continuity of the distribution of permafrost in zone I, zone II and zone III are 70%–80%, 50%–60% and 5%–30% respectively (Zhou and Guo, 1982). The vegetation types in zone I are similar to zone II, mainly coniferous forests and a small amount of grassland. The zone III includes many types of vegetation, mainly coniferous forest, broad-leaved forest, grassland and cropland.

### 2.2 Land cover data

The vegetation data come from the '1 : 1 million Chinese vegetation atlas', compiled by the Chinese Vegetation Atlas Editing Committee of the Chinese Academy of Sciences in 2001 (<http://www.nsii.org.cn/mapvege>) and were used to analyze and discuss the agreement and discrepancies in vegetation phenology (Fig. 1). The northeastern permafrost regions have high vegetation coverage, and the main vegetation type is forest, which is mostly distributed in the Da Hinggan Mountains and Xiao Hinggan Mountains. The main vegetation type in the Hulun Buir Plateau is grassland, and cultivated vegetation is scattered, mainly observed in the Songnen Plain. The vegetation types in the study area also include scattered shrubs, meadows, and swamps.

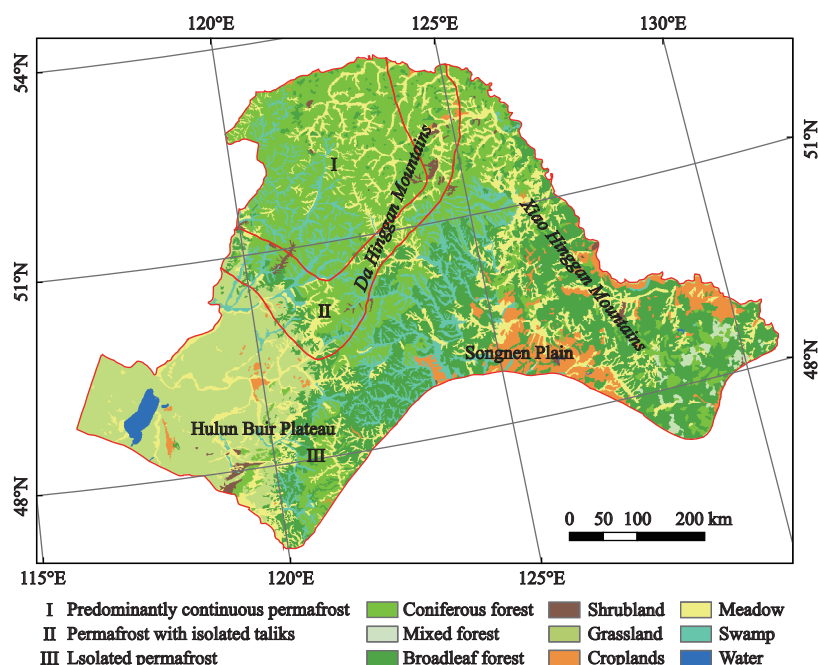


Fig. 1 Vegetation types in permafrost regions of the northeastern China

### 2.3 MODIS products

MODIS, carried on the two satellites Terra and Aqua, is an important instrument for observing global biological and physical processes. Many MODIS products of different time and space scales have been released on the official website (<https://search.earthdata.nasa.gov>). In this study, we used the MODIS 13Q1 datasets from 2000 to 2018 to derive SOS and EOS across the study area. MOD13Q1 is a MODIS three-level grid data product using the sinusoidal projection method. It has been systematically corrected according to the influence of the atmosphere and terrain. NDVI and EVI were extracted from MOD13Q1, with 250 m spatial resolution and a 16-d composite. After performing spatial operations such as mosaic, masking, and projection in ArcGIS, time series data of NDVI and EVI were obtained.

### 2.4 OCO-2 data

The Carbon Observation Satellite 2 (OCO-2) was launched in July 2014, with the primary task of collecting space-based global measurements of atmospheric CO<sub>2</sub> column mixing ratios (Luo et al., 2004). The revisit period is 16 d, the equatorial transit time is 13:30, and the global scale data are acquired every day. The discontinuous dataset of each ground pixel is  $1.3 \times 2.25 \text{ km}^2$ . In this study, the SIF data used the OCO-2 satellite's secondary product OCO-2\_L2\_Lite\_SIF.8r, which is based on the filling of the solar Fraunhofer line in narrow spectral windows of 757 nm and 771 nm, namely SIF<sub>757</sub> and SIF<sub>771</sub>. Compared with SIF<sub>771</sub>, SIF<sub>757</sub> has a good consistency with the gross primary productivity (GPP) observed by the carbon flux tower in monitoring phenology and seasonal changes (Li et al., 2018), and SIF<sub>757</sub> is considered to have higher retrieval accuracy than SIF<sub>771</sub> (Frankenberg et al., 2014). Thus, this study used SIF<sub>757</sub> to derive phenological metrics. OCO-2 SIF data are stored in Network Common Data Form (NetCDF) and converted to Shapefile format using R software. To ensure consistency with the time resolution of NDVI and EVI, the 16-d SIF data are combined into one period in ArcGIS, with 23 periods per year from 2015 to 2019.

### 2.5 Time series data smoothing

Due to the influence of clouds, atmosphere, and other factors (Goward et al., 1991; Tucker et al., 2005), the original data have different levels of outliers and noise,

which can lead to errors in the extraction of phenological metrics (Shen et al., 2013). Data smoothing is a method of removing noise from time series data while maintaining phenological information. Savitzky–Golay filtering (S–G) is based on local polynomial least squares, proposed by Savitzky and Golay (Savitzky and Golay, 1964). The formula is as follows (Equ. 1):

$$y_j^* = \frac{\sum_{i=-m}^{i=m} w_i \times y_{j+i}}{N} \quad (1)$$

where  $y_j^*$  is the filtered data,  $j$  represents the original coordinates of the sliding window,  $i$  represents the  $i$ th variable in the sliding window,  $y_{j+i}$  represents the original time series data,  $w_i$  is the filter coefficient, which represents the weight of the  $i$ th value that the filter starts,  $m$  is the size of the filter window, and  $N$  is the sliding window, the value of which is  $2m+1$ .

The NDVI, EVI, and SIF datasets were smoothed by the S–G filtering method in the TIMESAT software (Jönsson and Eklundh, 2004), which has been widely used for time series smoothing of satellite data (Boyd et al., 2011; Stanimirova et al., 2019).

### 2.6 SOS and EOS extraction

Common methods for phenological metrics extraction include threshold, moving average, curvature change rate, harmonic analysis, maximum slope, and inflection point methods. Among these, threshold methods are commonly applied for extracting phenological metrics by setting a certain threshold on the time series, which includes the fixed threshold (Lloyd, 1990) and dynamic threshold methods (Jonsson and Eklundh, 2002). The former is more effective for extracting phenological metrics of plants in specific areas but can not be applied to areas with different land cover types and soil backgrounds, and the latter is not subject to this limitation. This study uses the dynamic threshold method to derive key phenological metrics, including SOS and EOS. We applied 30% as the dynamic threshold, which was successfully used in previous studies in northeastern China (Zhao et al., 2016; Fu et al., 2018).

### 2.7 Investigating trends in SOS and EOS

The Mann–Kendall (MK) trend test method is a classic non-parametric trend test method proposed by Mann and Kendall (Irwin, 1934; Mann, 1945). In trend analysis,

is, the MK test can effectively detect the change trend of time series data without the sample following a specific distribution and without interference from a small number of outliers (Tabari et al., 2011). It is suitable for trend analysis of non-normal data such as phenology and precipitation data. Sen's slope is a non-parametric test method proposed and developed by Sen (Sen, 1968). It is often used to monitor the magnitude of the change trend of long-term series datasets. The calculation formula is as follows (Equ. 2):

$$Q = \text{median} \left( \frac{X_j - X_i}{j - i} \right) \quad 1 \leq i < j \leq n \quad (2)$$

where  $Q$  represents the Sen's slope,  $X_j$  and  $X_i$  represent the sequence value at time  $j$  and  $i$ , respectively, and the median is calculated based on all pairs of observations in the time series.

The combination of Sen's slope and the MK trend test has been widely used in vegetation trend analysis and is an important method for long-term series data analysis (Gocic and Trajkovic, 2013). In this study, the MK trend test method was used to analyze the change trend of vegetation phenology, and Sen's slope was used to quantify the change trend of phenology.

### 3 Results

#### 3.1 Results of time series data smoothing

Due to the time limit of SIF data, we calculated the average values of NDVI, EVI, and SIF in the study area and three subdivisions (zones I, II, and III) during 2015–2019. Fig. 2 provides an example of the original SIF data and the smoothing SIF time series using the S–G filtering method. This shows that the time series curve after S–G filtering is similar to the original curve shape fluctuation characteristics, with the outliers eliminated and smoother than the original curve, which is very important for accurate extraction of phenology information.

The results of filtered NDVI, EVI, and SIF curves in the whole area and zones I, II, and III are shown in Fig. 3. They show a constant seasonal change, the value increases after entering the growing season and decreases after the end of the growing season. In the whole area (Fig. 3a), the characteristics of the three curves were different. The SIF value began to dip at the beginning of the year and reached its lowest point in early

April. After approaching the growing season, it rose quickly, reaching its highest value in June, then dropped rapidly, which is different from NDVI and EVI. The NDVI value was higher than that of EVI, and the peak of EVI was somewhat sharper than that of NDVI. It is clear that the index characteristics of NDVI, EVI, and SIF in the whole area (Fig. 3a) are mostly consistent with the three sub-areas (Figs. 3b–d).

#### 3.2 Phenology metrics extraction results

The values of SOS extracted by NDVI ( $\text{SOS}_{\text{NDVI}}$ ), EVI ( $\text{SOS}_{\text{EVI}}$ ), and SIF ( $\text{SOS}_{\text{SIF}}$ ) as well as those of EOS extracted by NDVI ( $\text{EOS}_{\text{NDVI}}$ ), EVI ( $\text{EOS}_{\text{EVI}}$ ), and SIF ( $\text{EOS}_{\text{SIF}}$ ) in the whole area and three sub-areas are shown in Fig. 4. From 2015 to 2019,  $\text{SOS}_{\text{NDVI}}$  was between Julian day 110 and 126 in the whole area (Fig. 4a).  $\text{EOS}_{\text{NDVI}}$  had a small range of change, with a minimum value of Julian day 302 and a maximum value of Julian day 312 (Fig. 4b).  $\text{SOS}_{\text{EVI}}$  ranged from Julian day 126 to 134,  $\text{EOS}_{\text{EVI}}$  was basically unchanged, and fluctuated slightly from Julian day 282 to 290.  $\text{SOS}_{\text{SIF}}$  was smaller than  $\text{SOS}_{\text{NDVI}}$  and  $\text{SOS}_{\text{EVI}}$ , with a range of Julian day 136 to 143, and  $\text{EOS}_{\text{SIF}}$  ranged from Julian day 264 to 278. The phenological characteristics of zones I, II, and III based on NDVI, EVI and SIF are the same as the characteristics of the whole area (Figs. 4c–h), that is,  $\text{EOS}_{\text{SIF}}$  is the smallest,  $\text{EOS}_{\text{EVI}}$  is in the middle, and  $\text{EOS}_{\text{NDVI}}$  is the largest.

To further analyze the phenological inversion results of NDVI, EVI, and SIF, this study calculates the length of season (LOS), which is defined as the difference between EOS and SOS from 2015 to 2019 (Fig. 5). The  $\text{LOS}_{\text{NDVI}}$  ranges from Julian day 178 to 202 with an average value of 188,  $\text{LOS}_{\text{EVI}}$  is between Julian day 152 and 161 with an average value of 156, and  $\text{LOS}_{\text{SIF}}$  is

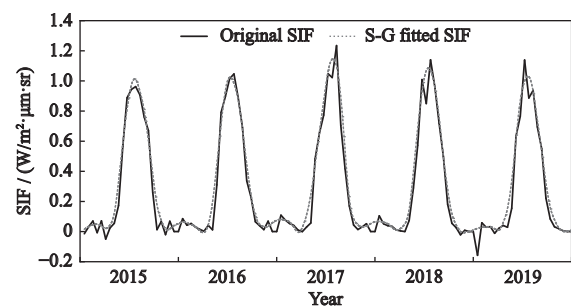
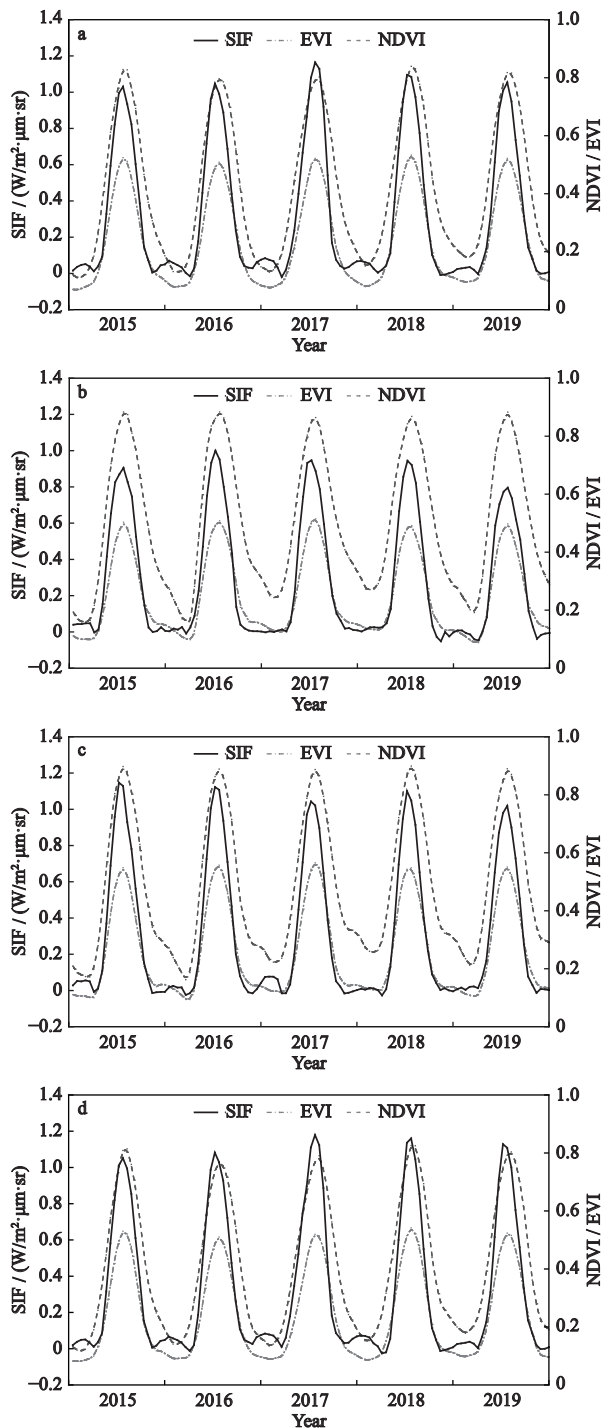


Fig. 2 Comparison of the solar-induced chlorophyll fluorescence (SIF) before and after Savitzky–Golay (S–G) filtering during 2015–2019 in permafrost regions of the northeastern China



**Fig. 3** Normalized difference vegetation index (NDVI), enhanced vegetation index (EVI), and solar-induced chlorophyll fluorescence (SIF) time series filtering curve of the whole area (a); zone I (b); zone II (c); and zone III (d) during 2015–2019 in permafrost regions of the northeastern China

between Julian day 128 and 135, with an average value of 130 in the whole area (Fig. 5a). Fig. 5 more intuitively reflects that the length of the growing season ex-

tracted by NDVI was the longest, followed by EVI, and then SIF.

### 3.3 Spatial patterns of vegetation phenology

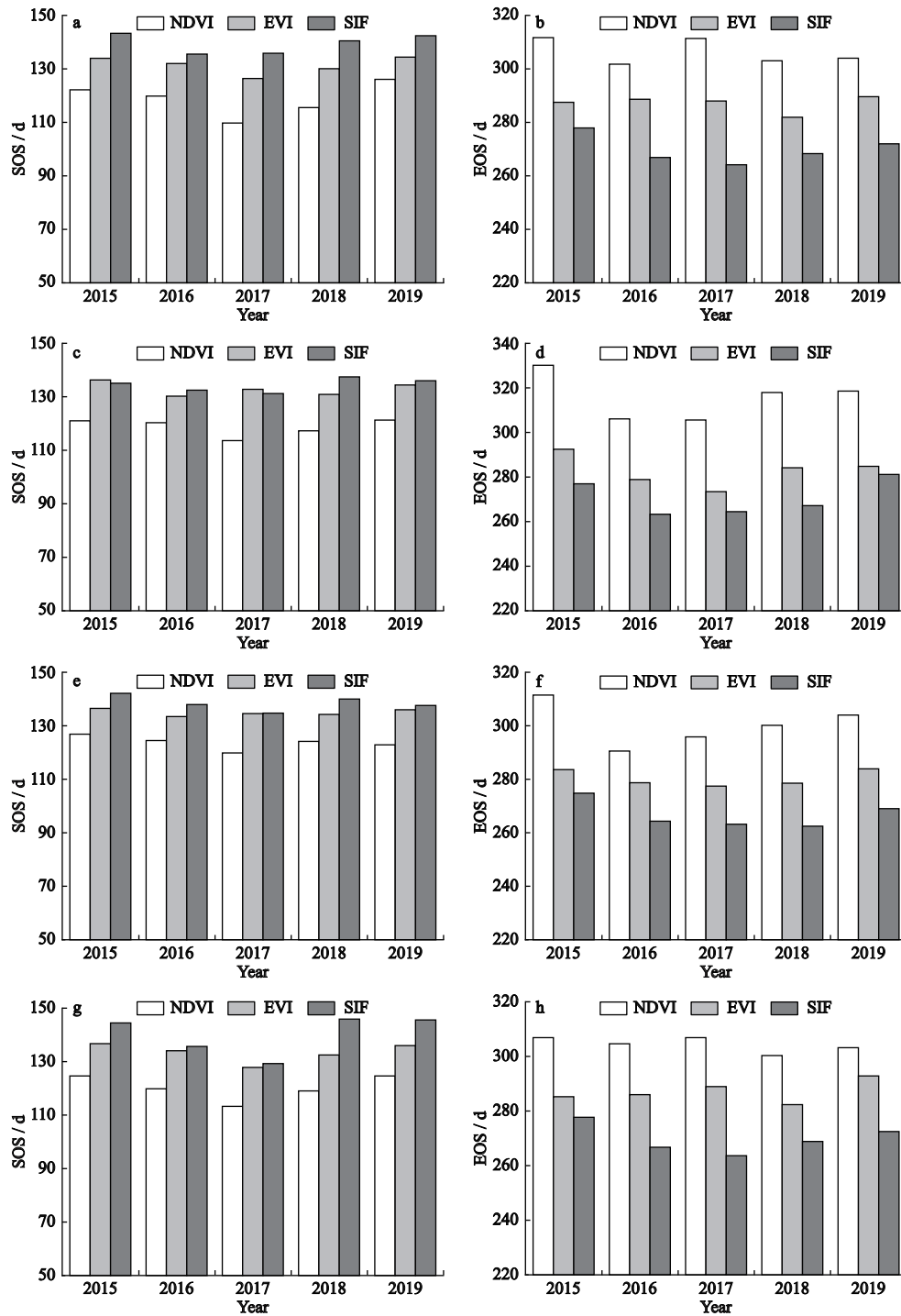
Phenological metrics and its change trends based on NDVI and EVI in different permafrost zones were calculated to understand the phenological characteristics of this area. The average values of  $SOS_{NDVI}$ ,  $SOS_{EVI}$ ,  $EOS_{NDVI}$ , and  $EOS_{EVI}$  were calculated for each pixel from 2000 to 2018 (Fig. 6).

The phenology values results based on NDVI and EVI are quite different. The average value of  $SOS_{NDVI}$  is concentrated from Julian day 80 to 112, from late March to late April, accounting for 97.8% of the total area (Fig. 6a). The  $SOS_{NDVI}$  value of the Hulun Buir Plateau, Songnen Plain, and zone I is smaller than that of the other regions.  $EOS_{NDVI}$  is concentrated around Julian day 288 to 336, accounting for 89.3% of the total area (Fig. 6c). The largest value of  $EOS_{NDVI}$  is mostly found in the forest areas of the Da Hinggan Mountains and Xiao Hinggan Mountains. The phenological metrics extracted by EVI are very different from the NDVI values.  $SOS_{EVI}$  is between Julian day 96 and 144, accounting for 96% of the total area (Fig. 6b). The  $SOS_{EVI}$  of the Hulun Buir Plateau and zone I is smaller than that in other areas.  $EOS_{EVI}$  is between Julian day 272 and 320, accounting for 97.8% of the total area (Fig. 6d). It is not difficult to find that  $SOS_{EVI}$  is larger than  $SOS_{NDVI}$ , and  $EOS_{EVI}$  is smaller than  $EOS_{NDVI}$ .

We separately calculated the average values of phenological metrics in zone I, zone II, and zone III (Table 1). The results show that the average values of  $SOS_{NDVI}$  are generally smaller than  $SOS_{EVI}$  and  $EOS_{NDVI}$  is larger than  $SOS_{EVI}$  in the three sub-areas. The average values of  $SOS_{NDVI}$  and  $SOS_{EVI}$  all showed that zone II was the largest, followed by zone I, and then zone III. The average values of  $EOS_{NDVI}$  and  $EOS_{EVI}$  all showed that zone I was the largest, followed by zone II, and then zone III.

### 3.4 Spatial phenology trends

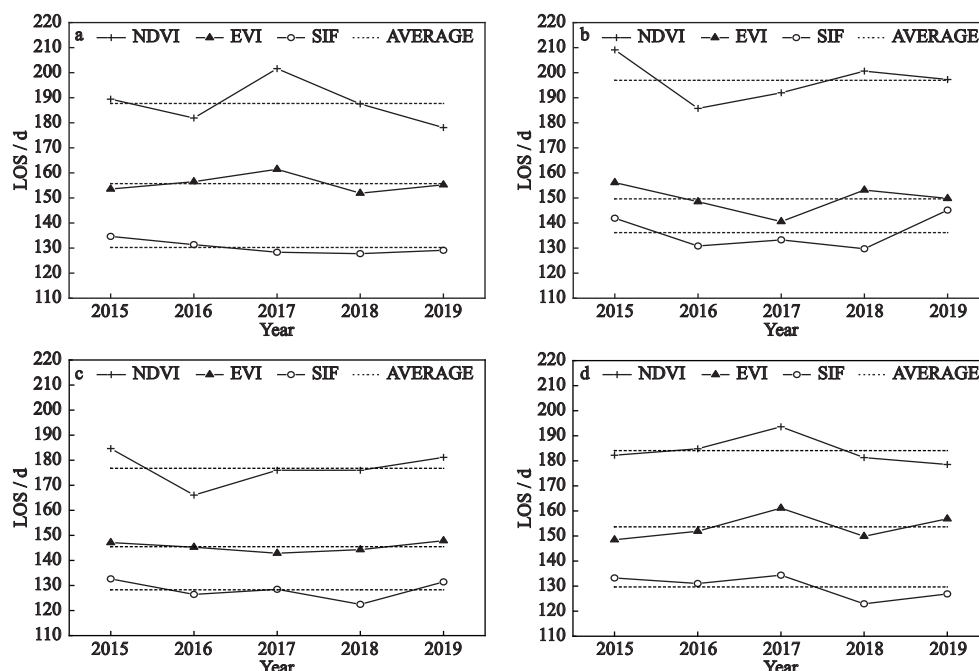
The Sen's slope and corresponding  $P$  values of  $SOS$  and  $EOS$  in the study area from 2000 to 2018 were calculated, and the significant pixels ( $P < 0.05$ ) are shown in Fig. 7. The  $SOS_{NDVI}$  change trend ranged from 6.4 d ahead to 6.0 d delayed over the study area, primarily showing an advancing trend. In the coniferous forest and grassland transitional area, broadleaved forest inter-



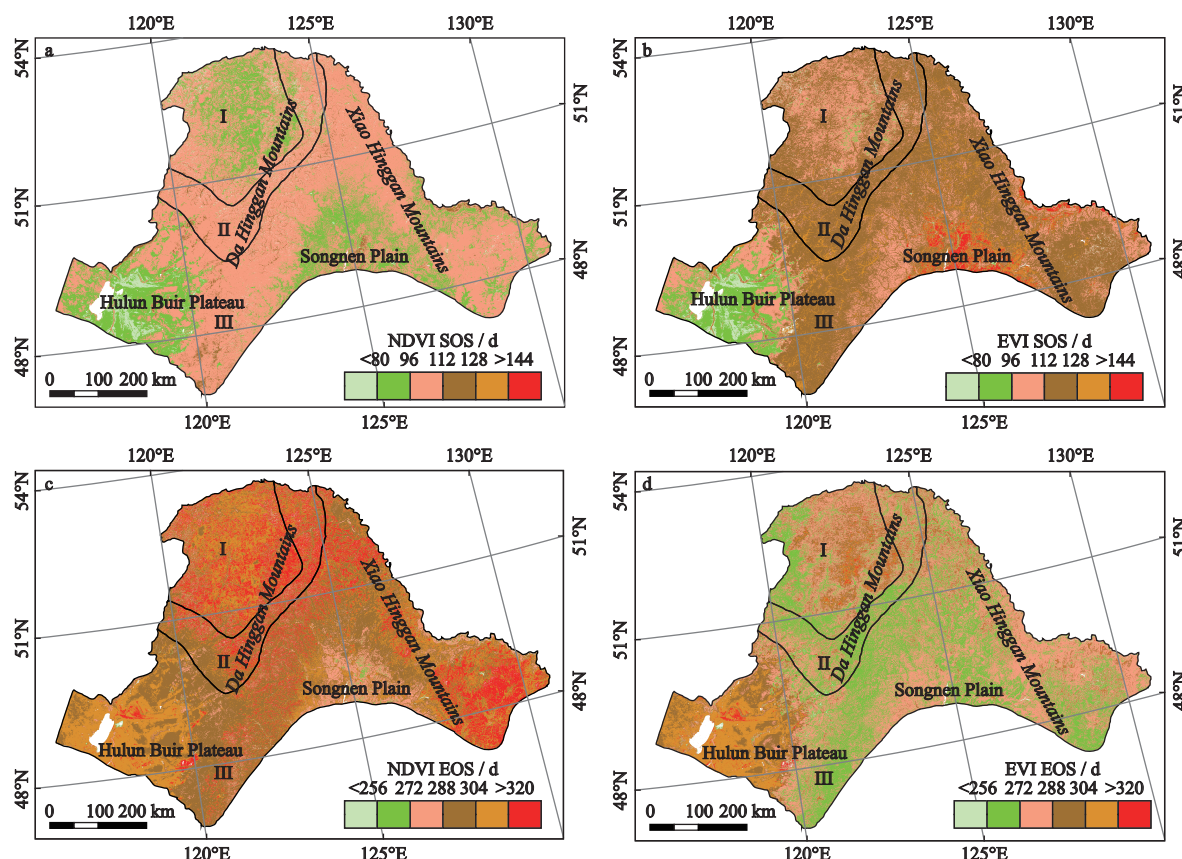
**Fig. 4** Normalized difference vegetation index (NDVI), enhanced vegetation index (EVI), and solar-induced chlorophyll fluorescence (SIF) phenological inversion results of the whole and three sub-areas during 2015–2019 in permafrost regions of the northeastern China. (a) start of growing season (SOS) in the whole area; (b) end of growing season (EOS) in the whole area; (c) start of growing season (SOS) in zone I; (d) end of growing season (EOS) in zone I; (e) start of growing season (SOS) in zone II; (f) end of growing season (EOS) in zone II; (g) start of growing season (SOS) in zone III; and (h) end of growing season (EOS) in zone III

leaved area, and zone I, the advance trend is more obvious, and a small part of SOS is delayed in the Hulun Buir Plateau. The  $EOS_{NDVI}$  change trend ranged from

8.0 d ahead and 9.2 d delayed over the past nearly 20 yr, with the delayed trend dominating. The  $EOS_{NDVI}$  in the Hulun Buir Plateau and the Songnen Plain in the study



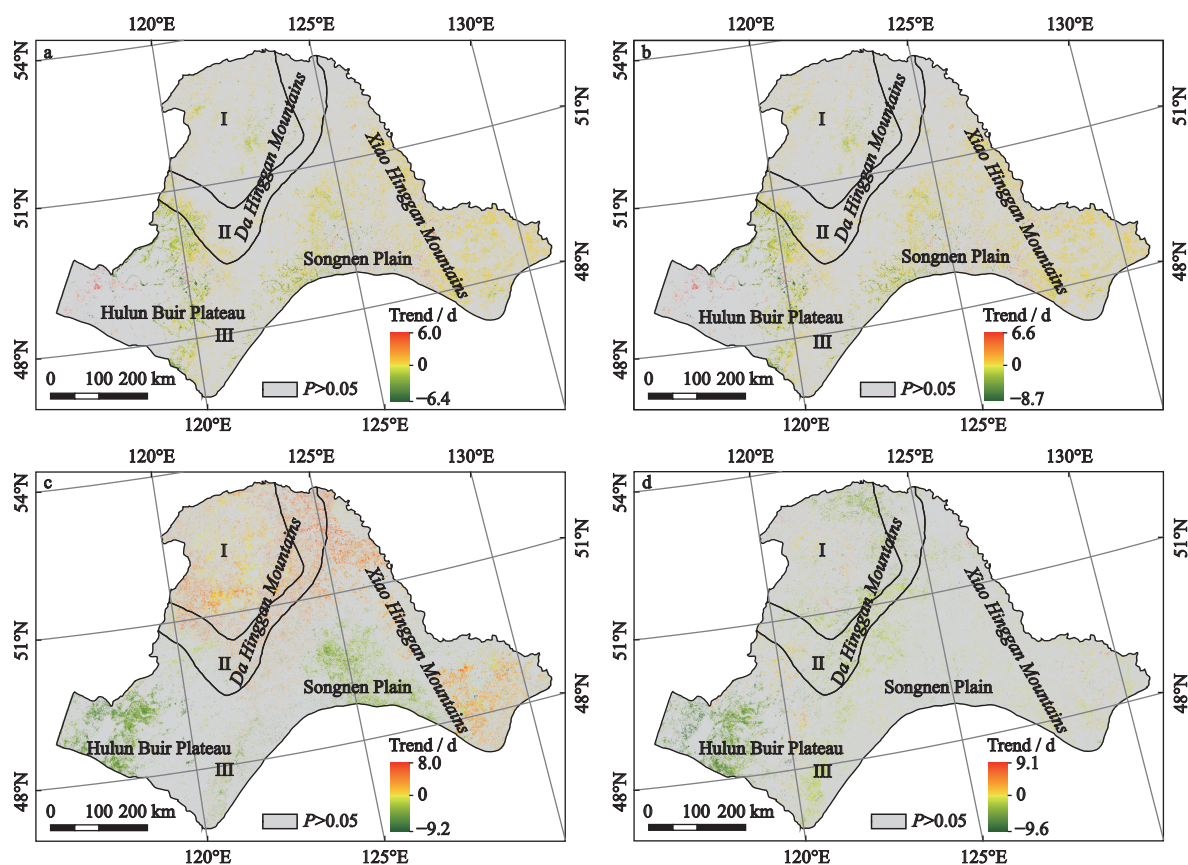
**Fig. 5** Results of length of growing season (LOS) and its average values in the whole area (a), zone I (b), zone II (c), and zone III (d) during 2015–2019 in permafrost regions of the northeastern China



**Fig. 6** The average of start of growing season (SOS) and end of growing season (EOS) during 2000–2018 in permafrost regions of northeastern China. (a) SOS extracted by normalized difference vegetation index (SOS<sub>NDVI</sub>); (b) SOS extracted by enhanced vegetation index (SOS<sub>EVI</sub>); (c) EOS extracted by normalized difference vegetation index (EOS<sub>NDVI</sub>); and (d) EOS extracted by enhanced vegetation index (EOS<sub>EVI</sub>)

**Table 1** Average values of the phenological parameters and the change trends in zone I, zone II, and zone III during 2000–2018 in permafrost regions of the northeastern China

Phenological metrics	Zone	Average values / d	Average values of change trends / d
SOS <sub>NDVI</sub>	I	95.15	−1.31
	II	99.34	−1.18
	III	78.79	−0.94
SOS <sub>EVI</sub>	I	116.27	−1.19
	II	123.90	−1.28
	III	94.55	−1.09
EOS <sub>NDVI</sub>	I	312.42	3.25
	II	308.21	3.87
	III	283.25	1.17
EOS <sub>EVI</sub>	I	286.60	−0.32
	II	280.72	−0.75
	III	259.08	−0.85

**Fig. 7** The change trend of start of growing season (SOS) and end of growing season (EOS) during 2000–2018 in permafrost regions of northeastern China (a) SOS extracted by normalized difference vegetation index (SOS<sub>NDVI</sub>); (b) SOS extracted by enhanced vegetation index (SOS<sub>EVI</sub>); (c) EOS extracted by normalized difference vegetation index (EOS<sub>NDVI</sub>); and (d) EOS extracted by enhanced vegetation index (EOS<sub>EVI</sub>)

area show a clear advancing trend, while the coniferous and broadleaved mixed forest areas in the east and the

northern coniferous forest area mainly show a postponed trend. The range of SOS<sub>EVI</sub> change trend was 8.7 d

ahead to 6.6 d delayed, primarily showing an advancing trend. The range of  $\text{EOS}_{\text{EVI}}$  change trend was 9.6 d ahead to 9.1 d delayed, with the advanced trend dominating. The advanced trend in the Hulun Buir grassland area is the most obvious.

The average values of change trends of phenological metrics in the subdivisions are shown in Table 1. The results show that  $\text{SOS}_{\text{NDVI}}$  and  $\text{SOS}_{\text{EVI}}$  are both negative, indicating that the overall SOS change trend of the subdivisions is advanced. There is a big difference between  $\text{EOS}_{\text{NDVI}}$  and  $\text{EOS}_{\text{EVI}}$ . The trend value of  $\text{EOS}_{\text{NDVI}}$  is positive, indicating that EOS is delayed, while  $\text{EOS}_{\text{EVI}}$  is negative, showing the opposite trend.

## 4 Discussion

### 4.1 Spatial phenology extraction using MODIS products

Some studies have used different methods and data to extract the phenological metrics of vegetation in northeastern China. Tang et al. (2015) estimated SOS and EOS in the Da Hinggan Mountains from 1982 to 2012 and showed that SOS were mainly distributed between Julian day 90 and 150, and the EOS ranged from Julian day 245 to 305. Yu et al. (2017) calculated the SOS in northeastern China from 1982 to 2015 ranging from the Julian day 100 to 140, and the EOS ranged from the Julian day 280 to 320. Liu et al. (2016) calculated the mean EOS values of temperate vegetation in China, and the results were mainly distributed from Julian day 270 to 310. Compared with these existing results, our results are basically consistent with them, and the phenology metrics derived from EVI are more accurate than NDVI. In addition, the smaller the pixel size, the greater the number of pure pixels, which could reduce the interference of mixed pixels on phenological extraction. The MODIS products we used with a pixel size of 250 m are more accurate than most existing studies.

Different cover types significantly affect the values of SOS and EOS. Yu et al. (2017) revealed that the change trend for each land cover type showed great diversity among different types. The difference in spatial characteristics between EVI and NDVI is that the phenological metrics extracted by EVI are more ‘fragmented’ than NDVI (Fig. 6). In other words, the extraction results of EVI are more consistent with vegetation types. One visible difference is in the Songnen Plain, which is covered

by cropland and broadleaf forests,  $\text{SOS}_{\text{NDVI}}$  and  $\text{EOS}_{\text{NDVI}}$  did not recognize the difference in phenology, while  $\text{SOS}_{\text{EVI}}$  and  $\text{EOS}_{\text{EVI}}$  recognized that the SOS of cultivated crops is later than that of broadleaf forests, and EOS is earlier than in broadleaf forests. Zhao et al. (2016) calculated the average values of the SOS and EOS in northeastern China and found that crops are significantly affected by sowing time and have SOS dates that are substantially later than those of other vegetation types, which is consistent with our conclusions.

The time series of NDVI and EVI can reflect the seasonal changes in vegetation and are used in monitoring vegetation phenology. However, as mentioned above, EVI is better than NDVI in terms of phenological extraction. The NDVI algorithm only uses red light and near-infrared bands, when the vegetation cover is high, the red-light band quickly saturates, resulting in a saturation effect (Huete et al., 2002). EVI has improved the algorithm design and synthesis, using the blue band and improving the post-processing of residual aerosols, reducing the influence of the atmosphere and soil background, and avoiding the problem of saturation in areas with high vegetation cover (Rocha and Shaver, 2009; Shen et al., 2014; Zhang et al., 2006).

Although NDVI and EVI are quite different in terms of phenological extraction, they have some similarities in space. For example, the average of  $\text{SOS}_{\text{NDVI}}$  and  $\text{SOS}_{\text{EVI}}$  in the Hulun Buir Plateau and zone I are earlier than other regions, and  $\text{EOS}_{\text{NDVI}}$  and  $\text{EOS}_{\text{EVI}}$  are later than other regions (Fig. 6). Therefore, LOS in the Hulun Buir Plateau and zone I are longer than in other regions, which is highly consistent with Yu et al. (2017).

### 4.2 Comparison of NDVI, EVI, and SIF filtering curves characteristics

The NDVI, EVI, and SIF curves present regular seasonal changes. The growth season values are much higher than those of the non-growth season and the growth season curves are roughly symmetrical. Many studies indicate that SIF meets the standards of extracting phenological metrics. For example, Jeong et al. (2017) concluded that continuing measurements from SIF and NDVI can help to comprehend the seasonal variations in vegetation structure, greenness, and physiology at large scales. Wang et al. (2019) used SIF to capture dryland vegetation phenology in the tropical arid region of North Australia and found that SIF has the potential to

improve the ability of dryland ecosystem phenology monitoring.

Fig. 3 shows that the curves of SIF change faster, the slope is large, and the duration of the growing season is the shortest. Compared with NDVI, SIF starts late and ends early; therefore, the length of the SIF growth season is much shorter than NDVI. SIF drops quickly after reaching the peak, which occurs earlier than EVI, the length of the SIF growing season is slightly shorter than that of the EVI, which is consistent with a previous study (Walther et al., 2016; Liu et al., 2018; Chang et al., 2019). We found that the characteristics of NDVI, EVI and SIF in a small study area are the same as those in a large area.

Five-year averages of the three indices were calculated separately to generate the mean curve (Fig. 8). The NDVI is clearly different from the other two datasets. It entered a rapid growth phase at the end of March, began to decay gradually until early August, and gradually declined in early October. The trends of the EVI and SIF curves were more consistent, and both began to rise rapidly at the end of April, but the SIF curve reached the peak of the growing season earlier in June, and then quickly decayed. The NDVI and EVI waveforms were very consistent. The difference is that the NDVI value was always higher than that of EVI, as EVI reduces the

influence of outliers, and its change range is lower than NDVI overall, and the change is relatively gentle (Shen et al., 2014). The EVI growing season starts late and ends early, and the overall distribution is concentrated.

#### 4.3 Advantages of SIF in extracting phenology

Compared with the vegetation indices, which reflect the greenness of vegetation, SIF, which reflects the characteristics of vegetation photosynthesis quickly and without damage, has become a 'probe' for monitoring the use of light energy by vegetation and can also reflect the true growth status of vegetation (Zarco-Tejada et al., 2013). In this study, SIF was used to extract phenology across the whole area and the three sub-areas and showed that the growing season length of SIF was significantly shorter than NDVI and EVI in phenological inversion, which is consistent with previous research (Chang et al., 2019). SIF has a strong physiological basis compared to NDVI and EVI and is directly linked to the biochemical processes of vegetation. Qiu et al. (2019) compared SIF and traditional VIs found that SIF are more consistent with GPP than those of VIs, suggesting the decoupling of photosynthesis and changes in greenness-based VIs. NDVI and EVI are both vegetation indices and reflect the greenness information of leaves and are affected by other factors such as back-

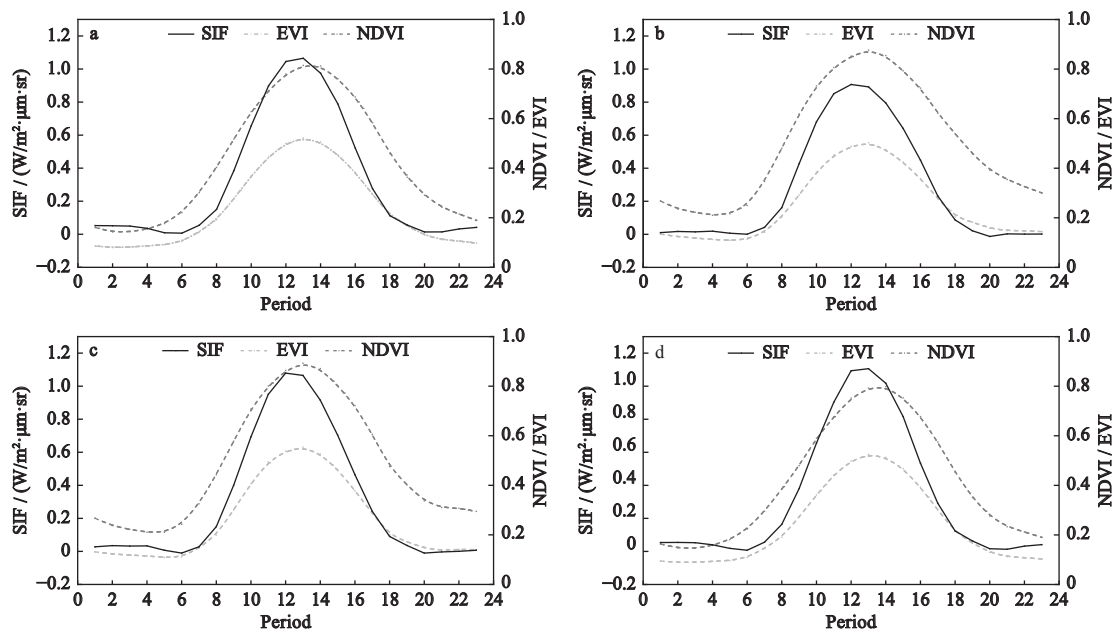


**Fig. 8** Average time series curve of normalized difference vegetation index (NDVI), enhanced vegetation index (EVI), and solar-induced chlorophyll fluorescence (SIF) in the whole area (a), zone I (b), zone II (c), and zone III (d) during 2015–2019 in permafrost regions of northeastern China

ground and high reflectivity of snow in winter, which leads to a decrease in NDVI and EVI. For example, after the snow and ice melt in spring, the greenness information has increased, but the vegetation has not entered the growing season. The trend of slow growth interfered with the extraction of phenology. Furthermore, the usual sign of the vegetation growth season is that the plant leaves begin to turn green and fall. However, the photosynthesis of plants before the leaves turn yellow or fall is very weak, and some evergreen coniferous forests also affect the changes in NDVI and EVI values (Gonsamo et al., 2012). Because of those, the phenological growth season based on SIF extraction starts late and ends early and is shorter than NDVI and EVI.

#### 4.4 Phenology of different permafrost zones

The permafrost regions of northeastern China can be divided into zones I, II, and III. It is generally believed that the process of permafrost degradation is from zone I to zone II and then zone III until it disappears. According to vegetation type data, we know that the vegetation types of permafrost zones I and II are basically the same, and zone III is not considered due to differences in vegetation types. Both the results of NDVI, EVI and SIF show that the length of the growing season in zone I is longer than that in zone II. We can assume that, as global climate change leads to the degradation of permafrost, the length of the growing season of the vegetation in the area will be shortened. The impact mechanism of permafrost degradation on vegetation is very complicated and needs to be further explored. Perhaps we can simply understand that permafrost is the most suitable growth environment for vegetation in permafrost regions such as *Larix gmelini*. When the permafrost is degraded, the vegetation temporarily does not adapt to this change, so the growing season becomes shorter.

#### 4.5 Study limitations

The short time span of SIF data and low spatial resolution are the main limitations of this study. Recently, many downscaled SIF data products have been produced (Zhang et al., 2018; Li and Xiao, 2019; Yu et al., 2019); however, these products are the result of spatial interpolation or fitting using other high-resolution data. They can not represent the real SIF due to errors.

Moreover, SIF data are spatially discontinuous point data, which is also a limitation for regional phenological extraction. Because the revisit period of the OCO-2 satellite is 16 d, the number of points in the study area is relatively small, and we use the average value of the points to represent the overall situation of the area. Sometimes, the area can not be accurately reflected owing to the sparse point data. With the development of remote sensing technology and the improvement of inversion methods, we believe that these problems will be solved.

## 5 Conclusions

With the development of various phenological observation technologies, the research of vegetation phenology has entered a stage that requires the integration of related disciplines and the use of new technologies. To explore the feasibility of applying SIF to extract phenological information in permafrost regions of northeastern China, this study uses SIF, NDVI, and EVI data to obtain the filtering time series curves and compares them with each other. We found that the growing season length of SIF is significantly shorter than NDVI and slightly shorter than EVI. Because the traditional vegetation indices, NDVI and EVI, reflect the phenology of leaves, which may be decoupled from actual photosynthesis and easily interfered with by the background. The permafrost regions of northeastern China are an ideal area for phenological research. This study derived the phenological metrics and change trends of the study area at the pixel scale and achieved good results. The length of the growing season in zone I is longer than that in zone II. Therefore, we predict that as zone I degenerates into zone II, the length of the vegetation growing season will become shorter.

As a new type of remote sensing technology, SIF can be used to extract vegetation phenology information, compensating for the shortcomings of traditional remote sensing vegetation indices. This is not only important for phenology development but also has a significant impact on understanding the response of ecosystems to global environmental changes.

## References

Baker N R, 2008. Chlorophyll fluorescence: a probe of photosyn-

- thesis *in vivo*. *Annual Review of Plant Biology*, 59(1): 89–113. doi: 10.1146/annurev.arplant.59.032607.092759
- Boyd D S, Almond S, Dash J et al., 2011. Phenology of vegetation in Southern England from Envisat MERIS terrestrial chlorophyll index (MTCI) data. *International Journal of Remote Sensing*, 32(23): 8421–8447. doi: 10.1080/01431161.2010.542194
- Bradley A V, Gerard F F, Barbier N et al., 2011. Relationships between phenology, radiation and precipitation in the Amazon region. *Global Change Biology*, 17(6): 2245–2260. doi: 10.1111/j.1365-2486.2011.02405.x
- Chang Q, Xiao X M, Jiao W Z et al., 2019. Assessing consistency of spring phenology of snow-covered forests as estimated by vegetation indices, gross primary production, and solar-induced chlorophyll fluorescence. *Agricultural and Forest Meteorology*, 275: 305–316. doi: 10.1016/j.agrformet.2019.06.002
- Cleland E E, Chuine I, Menzel A et al., 2007. Shifting plant phenology in response to global change. *Trends in Ecology & Evolution*, 22(7): 357–365. doi: 10.1016/j.tree.2007.04.003
- Delbart N, Le Toan T, Kergoat L et al., 2006. Remote sensing of spring phenology in boreal regions: a free of snow-effect method using NOAA-AVHRR and SPOT-VGT data (1982–2004). *Remote Sensing of Environment*, 101(1): 52–62. doi: 10.1016/j.rse.2005.11.012
- Deng G R, Zhang H Y, Guo X Y et al., 2019. Asymmetric effects of daytime and nighttime warming on boreal forest spring phenology. *Remote Sensing*, 11(14): 1651. doi: 10.3390/rs11141651
- Frankenberg C, Butz A, Toon G C, 2011. Disentangling chlorophyll fluorescence from atmospheric scattering effects in O<sub>2</sub> A-band spectra of reflected sun-light. *Geophysical Research Letters*, 38(3): L03801. doi: 10.1029/2010GL045896
- Frankenberg C, O'Dell C, Berry J et al., 2014. Prospects for chlorophyll fluorescence remote sensing from the Orbiting Carbon Observatory-2. *Remote Sensing of Environment*, 147: 1–12. doi: 10.1016/j.rse.2014.02.007
- Fu Y H, Piao S L, de Beeck M O et al., 2014. Recent spring phenology shifts in western Central Europe based on multiscale observations. *Global Ecology & Biogeography*, 23(11): 1255–1263. doi: 10.1111/geb.12210
- Fu Y Y, He H S, Zhao J J et al., 2018. Climate and spring phenology effects on autumn phenology in the Greater Khingan Mountains, Northeastern China. *Remote Sensing*, 10(3): 449. doi: 10.3390/rs10030449
- Gocic M, Trajkovic S, 2013. Analysis of changes in meteorological variables using Mann-Kendall and Sen's slope estimator statistical tests in Serbia. *Global and Planetary Change*, 100: 172–182. doi: 10.1016/j.gloplacha.2012.10.014
- Gonsamo A, Chen J M, Price D T et al., 2012. Land surface phenology from optical satellite measurement and CO<sub>2</sub> eddy covariance technique. *Journal of Geophysical Research: Biogeosciences*, 117: G03032. doi: 10.1029/2012JG002070
- Goward S N, Markham B, Dye D G et al., 1991. Normalized difference vegetation index measurements from the advanced very high resolution radiometer. *Remote Sensing of Environment*, 35(2-3): 257–277. doi: 10.1016/0034-4257(91)90017-Z
- Guanter L, Frankenberg C, Dudhia A et al., 2012. Retrieval and global assessment of terrestrial chlorophyll fluorescence from GOSAT space measurements. *Remote Sensing of Environment*, 121: 236–251. doi: 10.1016/j.rse.2012.02.006
- Guanter L, Zhang Y G, Jung M et al., 2014. Global and time-resolved monitoring of crop photosynthesis with chlorophyll fluorescence. *Proceedings of the National Academy of Sciences of the United States of America*, 111(14): E1327–E1333. doi: 10.1073/pnas.1320008111
- Guo M, Li J, Huang S B et al., 2020. Feasibility of using MODIS products to simulate sun-induced chlorophyll fluorescence (SIF) in boreal forests. *Remote Sensing*, 12(4): 680. doi: 10.3390/rs12040680
- Hmimina G, Dufrêne E, Pontailier J Y et al., 2013. Evaluation of the potential of MODIS satellite data to predict vegetation phenology in different biomes: an investigation using ground-based NDVI measurements. *Remote Sensing of Environment*, 132: 145–158. doi: 10.1016/j.rse.2013.01.010
- Huete A, Didan K, Miura T et al., 2002. Overview of the radiometric and biophysical performance of the MODIS vegetation indices. *Remote Sensing of Environment*, 83(1-2): 195–213. doi: 10.1016/S0034-4257(02)00096-2
- Irwin J O, 1934. Correlation methods in psychology. *British Journal of Psychology*, 25(1): 86–91. doi: 10.1111/j.2044-8295.1934.tb00727.x
- Jeong S J, Schimel D, Frankenberg C et al., 2017. Application of satellite solar-induced chlorophyll fluorescence to understanding large-scale variations in vegetation phenology and function over northern high latitude forests. *Remote Sensing of Environment*, 190: 178–187. doi: 10.1016/j.rse.2016.11.021
- Joiner J, Yoshida Y, Vasilkov A P et al., 2011. First observations of global and seasonal terrestrial chlorophyll fluorescence from space. *Biogeosciences*, 8(3): 637–651. doi: 10.5194/bg-8-637-2011
- Joiner J, Yoshida Y, Vasilkov A P et al., 2014. The seasonal cycle of satellite chlorophyll fluorescence observations and its relationship to vegetation phenology and ecosystem atmosphere carbon exchange. *Remote Sensing of Environment*, 152: 375–391. doi: 10.1016/j.rse.2014.06.022
- Jonsson P, Eklundh L, 2002. Seasonality extraction by function fitting to time-series of satellite sensor data. *IEEE Transactions on Geoscience and Remote Sensing*, 40(8): 1824–1832. doi: 10.1109/TGRS.2002.802519
- Jönsson P, Eklundh L, 2004. TIMESAT—a program for analyzing time-series of satellite sensor data. *Computers & Geosciences*, 30(8): 833–845. doi: 10.1016/j.cageo.2004.05.006
- Justice C O, Townshend J R G, Holben B N et al., 1985. Analysis of the phenology of global vegetation using meteorological satellite data. *International Journal of Remote Sensing*, 6(8): 1271–1318. doi: 10.1080/01431168508948281
- Köhler P, Guanter L, Kobayashi H et al., 2018. Assessing the po-

- tential of sun-induced fluorescence and the canopy scattering coefficient to track large-scale vegetation dynamics in Amazon forests. *Remote Sensing of Environment*, 204: 769–785. doi: 10.1016/j.rse.2017.09.025
- Lee J E, Frankenberg C, Van der Tol C et al., 2013. Forest productivity and water stress in Amazonia: observations from GOSAT chlorophyll fluorescence. *Proceedings of the Royal Society B: Biological Sciences*, 280(1761): 20130171. doi: 10.1098/rspb.2013.0171
- Li X, Xiao J F, He B B, 2018. Chlorophyll fluorescence observed by OCO-2 is strongly related to gross primary productivity estimated from flux towers in temperate forests. *Remote Sensing of Environment*, 204: 659–671. doi: 10.1016/j.rse.2017.09.034
- Li X, Xiao J F, 2019. A global, 005-degree product of solar-induced chlorophyll fluorescence derived from OCO-2, MODIS, and Reanalysis Data. *Remote Sensing*, 11(5): 517. doi: 10.3390/rs11050517
- Liu Q, Fu Y H, Zeng Z Z et al., 2016. Temperature, precipitation, and insolation effects on autumn vegetation phenology in temperate China. *Global Change Biology*, 22(2): 644–655. doi: 10.1111/gcb.13081
- Liu Xiaotian, Zhou Lei, Shi Hao et al., 2018. Phenological characteristics of temperate coniferous and broad-leaved mixed forests based on multiple remote sensing vegetation indices, chlorophyll fluorescence and CO<sub>2</sub> flux data. *Acta Ecologica Sinica*, 38(10): 3482–3494. (in Chinese)
- Lloyd D, 1990. A phenological classification of terrestrial vegetation cover using shortwave vegetation index imagery. *International Journal of Remote Sensing*, 11(12): 2269–2279. doi: 10.1080/01431169008955174
- Luo Y W, Su B, Currie W S et al., 2004. Progressive nitrogen limitation of ecosystem responses to rising atmospheric carbon dioxide. *BioScience*, 54(8): 731–739. doi: 10.1641/0006-3568(2004)054[0731:Pnloer]2.0.Co;2
- Mao Dehuang, Wang Zongming, Luo Ling et al., 2012. Dynamic changes of vegetation net primary productivity in permafrost zone of Northeast China in 1982–2009 in response to global change. *Chinese Journal of Applied Ecology*, 23(26): 1511–1519. (in Chinese)
- Mann H B, 1945. Nonparametric tests against trend. *Econometrica*, 13(3): 245–259. doi: 10.2307/1907187
- Meroni M, Rossini M, Guanter L et al., 2009. Remote sensing of solar-induced chlorophyll fluorescence: review of methods and applications. *Remote Sensing of Environment*, 113(10): 2037–2051. doi: 10.1016/j.rse.2009.05.003
- Mi Desheng, 1990. Map of snow, ice and frozen ground in China. *Journal of Glaciology and Geocryology*, 12(4): 175–181. (in Chinese)
- Myneni R B, Keeling C D, Tucker C J et al., 1997. Increased plant growth in the northern high latitudes from 1981 to 1991. *Nature*, 386(6626): 698–702. doi: 10.1038/386698a0
- Piao S L, Friedlingstein P, Ciais P et al., 2007. Growing season extension and its impact on terrestrial carbon cycle in the Northern Hemisphere over the past 2 decades. *Global Biogeochemical Cycles*, 21(3): GB3018. doi: 10.1029/2006gb002888
- Qiu B, Li W K, Wang X Q et al., 2019. Satellite-observed solar-induced chlorophyll fluorescence reveals higher sensitivity of alpine ecosystems to snow cover on the Tibetan Plateau. *Agricultural and Forest Meteorology*, 271: 126–134. doi: 10.1016/j.agrformet.2019.02.045
- Richardson A D, Anderson R S, Arain M A et al., 2012. Terrestrial biosphere models need better representation of vegetation phenology: results from the North American Carbon Program Site Synthesis. *Global Change Biology*, 18(2): 566–584. doi: 10.1111/j.1365-2486.2011.02562.x
- Richardson A D, Keenan T F, Migliavacca M et al., 2013. Climate change, phenology, and phenological control of vegetation feedbacks to the climate system. *Agricultural and Forest Meteorology*, 169: 156–173. doi: 10.1016/j.agrformet.2012.09.012
- Rocha A V, Shaver G R, 2009. Advantages of a two band EVI calculated from solar and photosynthetically active radiation fluxes. *Agricultural and Forest Meteorology*, 149(9): 1560–1563. doi: 10.1016/j.agrformet.2009.03.016
- Savitzky A, Golay M J E, 1964. Smoothing and differentiation of data by simplified least squares procedures. *Analytical Chemistry*, 36(8): 1627–1639. doi: 10.1021/ac60214a047
- Sen P K, 1968. Estimates of the regression coefficient based on Kendall's Tau. *Journal of the American Statistical Association*, 63(324): 1379–1389. doi: 10.1080/01621459.1968.10480934
- Shen M G, Sun Z Z, Wang S P et al., 2013. No evidence of continuously advanced green-up dates in the Tibetan Plateau over the last decade. *Proceedings of the National Academy of Sciences of the United States of America*, 110(26): E2329. doi: 10.1073/pnas.1304625110
- Shen M G, Tang Y H, Desai A R et al., 2014. Can EVI-derived land-surface phenology be used as a surrogate for phenology of canopy photosynthesis? *International Journal of Remote Sensing*, 35(3): 1162–1174. doi: 10.1080/01431161.2013.875636
- Stanimirova R, Cai Z Z, Melaas E K et al., 2019. An empirical assessment of the MODIS land cover dynamics and TIMESAT land surface phenology algorithms. *Remote Sensing*, 11(19): 2201. doi: 10.3390/rs11192201
- Tabari H, Somee B S, Zadeh M R, 2011. Testing for long-term trends in climatic variables in Iran. *Atmospheric Research*, 100(1): 132–140. doi: 10.1016/j.atmosres.2011.01.005
- Tang H, Li Z W, Zhu Z L et al., 2015. Variability and climate change trend in vegetation phenology of recent decades in the Greater Khingan Mountain area, Northeastern China. *Remote Sensing*, 7(9): 11914–11932. doi: 10.3390/rs70911914
- Tang J W, Körner C, Muraoka H et al., 2016. Emerging opportunities and challenges in phenology: a review. *Ecosphere*, 7(8): e01436. doi: 10.1002/ecs2.1436
- Tucker C J, Pinzon J E, Brown M E et al., 2005. An extended AVHRR 8-km NDVI dataset compatible with MODIS and SPOT vegetation NDVI data. *International Journal of Remote Sensing*, 26(20): 4485–4498. doi: 10.1080/01431160500168686

- Walther S, Voigt M, Thum T et al., 2016. Satellite chlorophyll fluorescence measurements reveal large-scale decoupling of photosynthesis and greenness dynamics in boreal evergreen forests. *Global Change Biology*, 22(9): 2979–2996. doi: 10.1111/gcb.13200
- Wang C, Beringer J, Hutley L B et al., 2019. Phenology dynamics of dryland ecosystems along the North Australian tropical transect revealed by satellite solar-induced chlorophyll fluorescence. *Geophysical Research Letters*, 46(10): 5294–5302. doi: 10.1029/2019GL082716
- Wang X, Dannenberg M P, Yan D et al., 2020. Globally consistent patterns of asynchrony in vegetation phenology derived from optical, microwave, and fluorescence satellite data. *Journal of Geophysical Research: Biogeosciences*, 125(7): e2020JG005732. doi: 10.1029/2020JG005732
- Wei Z, Jin H J, Zhang J M et al., 2011. Prediction of permafrost changes in Northeastern China under a changing climate. *Science China Earth Sciences*, 54(6): 924–935. doi: 10.1007/s11430-010-4109-6
- Wu C Y, Chen J M, Black T A et al., 2013. Interannual variability of net ecosystem productivity in forests is explained by carbon flux phenology in autumn. *Global Ecology and Biogeography*, 22(8): 994–1006. doi: 10.1111/geb.12044
- Wu C Y, Gonsamo A, Gough C M et al., 2014. Modeling growing season phenology in North American forests using seasonal mean vegetation indices from MODIS. *Remote Sensing of Environment*, 147: 79–88. doi: 10.1016/j.rse.2014.03.001
- Yu L, Wen J, Chang C Y et al., 2019. High-Resolution Global Contiguous SIF of OCO-2. *Geophysical Research Letters*, 46(3): 1449–1458. doi: 10.1029/2018GL081109
- Yu L X, Liu T X, Bu K et al., 2017. Monitoring the long term vegetation phenology change in Northeast China from 1982 to 2015. *Scientific Reports*, 7(1): 14770. doi: 10.1038/s41598-017-14918-4
- Yu Xinfang, Zhuang Dafang, 2006. Monitoring forest phenophases of Northeast China based on MODIS NDVI data. *Resources Science*, 28(4): 111–117. (in Chinese)
- Zarco-Tejada P J, Morales A, Testi L et al., 2013. Spatio-temporal patterns of chlorophyll fluorescence and physiological and structural indices acquired from hyperspectral imagery as compared with carbon fluxes measured with eddy covariance. *Remote Sensing of Environment*, 133: 102–115. doi: 10.1016/j.rse.2013.02.003
- Zhang X Y, Friedl M A, Schaaf C B, 2006. Global vegetation phenology from Moderate Resolution Imaging Spectroradiometer (MODIS): evaluation of global patterns and comparison with in situ measurements. *Journal of Geophysical Research: Biogeosciences*, 111: G04017. doi: 10.1029/2006JG000217
- Zhang Y, Joiner J, Alemohammad S H et al., 2018. A global spatially contiguous solar-induced fluorescence (CSIF) dataset using neural networks. *Biogeosciences*, 15(19): 5779–5800. doi: 10.5194/bg-15-5779-2018
- Zhao J J, Wang Y Y, Zhang Z X et al., 2016. The variations of land surface phenology in Northeast China and its responses to climate change from 1982 to 2013. *Remote Sensing*, 8(5): 400. doi: 10.3390/rs8050400
- Zhou Yuke, 2020. Analysis of controlling factors for vegetation productivity in Northeast China. *Acta Geographica Sinica*, 75(1): 53–67. (in Chinese)
- Zhou Youwu, Guo Dongxin, 1982. Principal characteristics of permafrost in China. *Journal of Glaciology and Geocryology*, 4(1): 1–19. (in Chinese)